

Proper Orthogonal Decomposition of Solar Photospheric Motions

A. Vecchio,¹ V. Carbone,¹ F. Lepreti,¹ L. Primavera,¹ L. Sorriso-Valvo,^{2,1} P. Veltri,¹ G. Alfonsi,³ and Th. Straus⁴

¹*Dipartimento di Fisica, Università della Calabria, and Istituto Nazionale di Fisica della Materia, Unità di Cosenza, 87030 Rende (CS), Italy*

²*Laboratorio Regionale LYCRYL - INFN/CNR, 87030 Rende (CS), Italy*

³*Dipartimento di Difesa del Suolo, Università della Calabria, 87030 Rende (CS), Italy*

⁴*INAF - Osservatorio Astronomico di Capodimonte, Napoli, Italy*

(Received 24 March 2005; published 3 August 2005)

The spatiotemporal dynamics of the solar photosphere is studied by performing a proper orthogonal decomposition (POD) of line of sight velocity fields computed from high resolution data coming from the MDI/SOHO instrument. Using this technique, we are able to identify and characterize the different dynamical regimes acting in the system. Low-frequency oscillations, with frequencies in the range 20–130 μHz , dominate the most energetic POD modes (excluding solar rotation), and are characterized by spatial patterns with typical scales of about 3 Mm. Patterns with larger typical scales of ≈ 10 Mm, are associated to p -modes oscillations at frequencies of about 3000 μHz .

DOI: [10.1103/PhysRevLett.95.061102](https://doi.org/10.1103/PhysRevLett.95.061102)

PACS numbers: 96.60.Mz, 92.60.Ek, 96.60.Ly

The solar photosphere is an interesting example of a system exhibiting complex spatiotemporal behavior, a quite common feature in a wide range of systems far from equilibrium. The early research in pattern formation focused on the presence of simple periodic structures, while the main questions currently addressed concern regimes characterized by higher complexity, that is, patterns that are more irregular in space and time. This is often related to the occurrence of intermediate states between order and turbulence [1]. High resolution images of the solar photosphere show that the whole surface of the sun is covered by a cellular pattern, the so-called *solar granulation*, consisting in bright cells (granules), with roughly 10^3 km size, surrounded by a dark background of intergranular lanes; cf. [2,3]. This structure represents the manifestation of the complex convective dynamics, at high Rayleigh numbers, occurring in the subphotospheric layers [3,4]. Other patterns are also observed in the photosphere, namely, the supergranulation ($\approx 3 \times 10^4$ km size) [5,6] and giant cells of size about 10^5 km, perhaps the result of global convection over the whole solar convective depth [7]. In the solar photosphere the convective dynamics coexist with the contribution of solar oscillations. The interior of the sun, because of the gravitational field and density stratification, behaves like a resonant cavity and supports the excitation of global oscillations [5,8,9]. Depending on the restoring force, two main types of waves can be excited, namely, acoustic high-frequency p modes [5,9] (in the range 1000–5000 μHz [10]) and gravitational low-frequency g modes [8,9] (in the range 1–200 μHz). The Fourier k - ω spectra of line of sight photospheric velocity fields show ridges corresponding to the discrete p modes [11] (see Fig. 2). On the other hand, discrete frequencies in the low-frequency range (g modes) are not recognized, but rather the power observed in this range is spread over a continuum, commonly attributed to the solar turbulent convection. Indications for the presence of

160 min discrete oscillations within a continuum have been reported [8], followed by contradictory evidences [12]. Despite these attempts, no unambiguous mode identification and classification has been established so far.

In the present Letter, we use the proper orthogonal decomposition (POD) as a powerful tool to investigate the dynamics of stochastic spatiotemporal fields. In astrophysical contexts, POD has been recently used to analyze the spatiotemporal dynamics of the solar cycle [13]. Introduced in the context of turbulence [14], the POD decomposes a field $u(\mathbf{r}, t)$ as

$$u(\mathbf{r}, t) = \sum_{j=0}^{\infty} a_j(t) \Psi_j(\mathbf{r}), \quad (1)$$

the eigenfunctions Ψ_j being constructed by maximizing the average projection of the field onto Ψ_j , constrained to the unitary norm. Averaging leads to an optimization problem that can be cast as

$$\int_{\Omega} \langle u(\mathbf{r}, \mathbf{t}), u(\mathbf{r}', \mathbf{t}) \rangle \Psi(\mathbf{r}') d\mathbf{r}' = \lambda \Psi(\mathbf{r}), \quad (2)$$

where Ω represents the spatial domain and brackets represent time averages. The integral Eq. (2) provides the eigenfunctions Ψ_j and a countable, infinite set of ordered eigenvalues $\lambda_j \geq \lambda_{j+1}$, each representing the kinetic energy of the j th mode. Thus, POD builds up the basis functions, which are not given *a priori*, but rather obtained from observations. The time coefficients $a_j(t)$ are then computed from the projection of the data on the corresponding basis functions $\Psi_j(\mathbf{r})$ so that the sum (1), when truncated to N terms, contains the largest possible energy with respect to any other linear decomposition of the same truncation order. The POD basis functions are optimal in turbulence with respect to the classical Fourier analysis, where the basis functions are not proper eigenfunctions of the signal. This method is particularly appropriate when

analyzing complex physical systems, where different dynamical regimes coexist. POD allows us to identify these regimes and to characterize their energetics and their spatial structure. We show that POD is able to capture the main aspects of the spatiotemporal dynamics of the solar photosphere.

The line of sight velocity fields $u(x, y, t)$ (x, y being the coordinates on the surface of the sun) used in this work have been obtained from images acquired by the Michelson Doppler Imager (MDI) instrument mounted on the SOHO spacecraft [15]. The image size is 695×695 pixels, with a spatial resolution of about 0.6 arcsec (1 arcsec ≈ 725 km on the surface). The time series spans

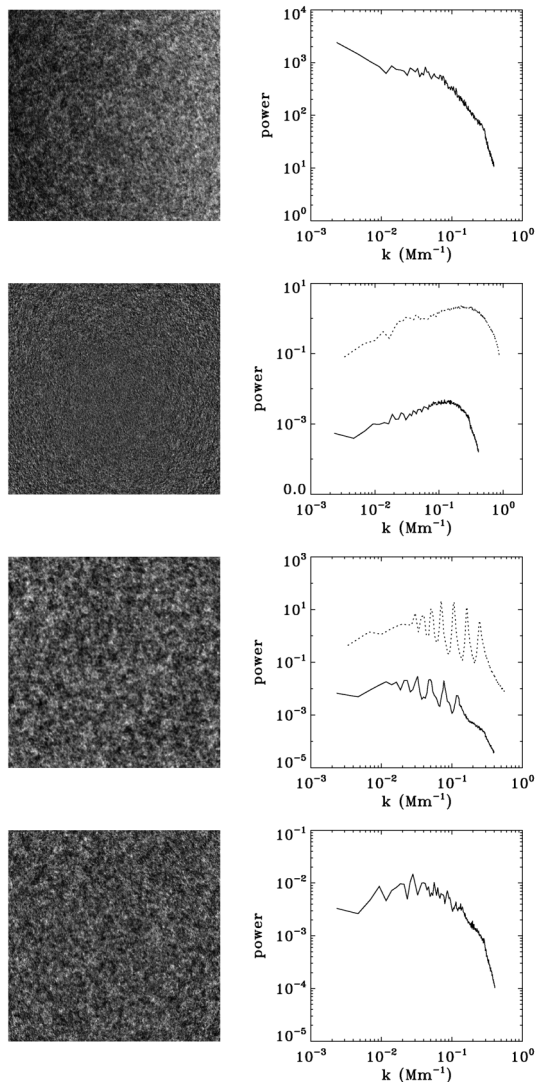


FIG. 1. Left column, from top to bottom: one snapshot of the original data, and the POD eigenfunctions $\Psi_j(x, y)$ in the plane (x, y) for the three modes $j = 8$, $j = 12$, and $j = 49$. Each image covers about $300 \times 300 \text{ Mm}^2$ on the solar surface. Right column: the wave vector spectra $|\Psi_j(k)|^2$ of the corresponding images. On the second and third spectra, the wave vector spectra obtained from the k - ω cut, respectively, at $\omega = 76 \mu\text{Hz}$ and $\omega = 3254 \mu\text{Hz}$, are superimposed (dotted lines, in arbitrary units).

a time interval $T = 886$ min, images being sampled every minute. The top panel of Fig. 1 shows one of the snapshots of the data set, together with its spatial spectrum. These data have been already studied in the past with Fourier techniques [16], and the k - ω power spectrum of the velocity signal is shown in Fig. 2.

The POD of the velocity field $u(x, y, t)$ yields a set of eigenfunctions $\Psi_j(x, y)$ and coefficients $a_j(t)$, as well as the sequence of eigenvalues λ_j ($j = 0, 1, \dots, 886$, sorted in decreasing energetic content). Most of the energy is associated with the first POD mode, accounting for the line of sight component of solar rotation. As this is neither the expression of solar turbulence nor oscillations, this first POD mode will be ignored throughout this Letter. The rest of the energy is decreasingly shared by the following 885 modes, so that, for example, only 4% is associated to the second ($j = 1$) POD mode. In laboratory turbulent flows, POD attribute almost 90% of total energy to the typical large-scale coherent structures, confined to $j \leq 2$ [17]. In our case, 90% of energy (excluding the rotation) is contained in the first 140 modes. This indicates the absence of dominating large-scale structures and the presence of some turbulent dynamics related to nonlinear interactions among different modes and structures at all scales.

We now turn the attention to the eigenfunctions, namely, the spatial patterns, found by POD, and reported in Fig. 1 for three modes. The power spectra $|\Psi_j(k)|^2$ obtained from Fourier transform of the eigenfunctions $\Psi_j(x, y)$ are also reported in Fig. 1, for the same three modes, as a function of the wave vector $k = (k_x^2 + k_y^2)^{1/2}$. It can be observed that the patterns are rather disordered, with a broad spectrum. Moreover, modes can be separated in three different groups, accordingly to grain size, as is shown in Fig. 1. The $1 \leq j \leq 11$, most energetic modes display a pattern

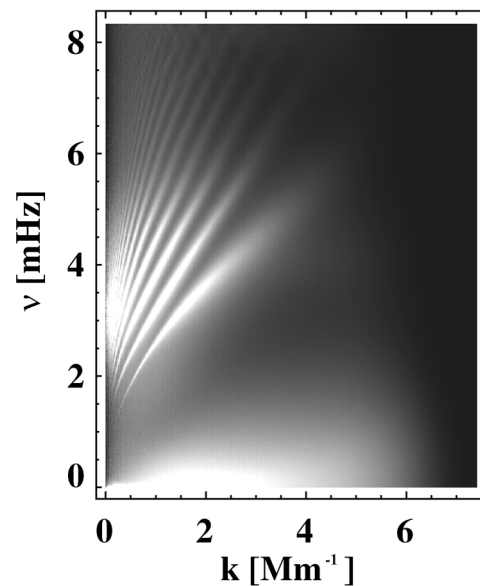


FIG. 2. The k - ω spectrum of the data set.

with very fine structures, recalling the photospheric granulation, with a broad spectrum indicating the complex nature of the POD modes, and show a center-limb modulation. Conversely, eigenfunctions of the modes $j = 12$ and $j = 13$ present a coarser pattern, and their (still broad) spectra show a number of ridges. The further lower energy modes cannot be precisely classified, and seem to present a mixture of the previous characteristics, both in grain size and in spectral shape. The spatial pattern associated to each mode, although complicated, can be quantitatively characterized by computing the integral scale length $L_j = \int_0^\infty |\psi_j(k)|^2 k^{-1} dk / \int_0^\infty |\psi_j(k)|^2 dk$ which represents the energy containing scale of classical turbulence [18]. This allows us to estimate the typical scale for the first ten fine grained modes $L \approx 3$ Mm, while for the coarse grained modes $L \approx 10$ Mm.

The eigenfunctions described above are associated with the corresponding coefficients, accounting for the temporal evolution of each mode. In Fig. 3 we report, for the same modes represented in Fig. 1, the time behavior of the coefficients $a_j(t)$, together with their Fourier spectra $|a_j(\nu)|^2$. As can be seen, for all the eigenfunctions the spectra of the time coefficients present two peaks, located in two well-defined and separated frequency ranges. The fine grained eigenfunctions (e.g., $j = 8$) are associated with time coefficients dominated by low-frequency oscillations. For the coarse grained patterns (e.g., $j = 12$) the high-frequency peak becomes of the same order, and even

slightly higher than the low-frequency one. For the intermediate cases (e.g., $j = 49$), the amplitudes of the two peaks are again of the same order, but with weak prevalence of the low frequencies. For each POD mode, the high-frequency peaks can be identified from the spectra, lying in the range 3250–3550 μHz . In a similar way, for the low-frequency oscillations, we find frequencies in the range 20–127 μHz .

We try now to understand the results observed with POD. Let us first focus on the high-frequency modes. Both the information on the involved spatial scales and the measured frequencies indicate that solar p -mode contributions are identified by POD. Indeed, the frequencies we obtain (for instance, $\nu = 3405$ μHz for $j = 12$, $\nu = 3367$ μHz for $j = 13$) are compatible with the p modes observed using Fourier techniques [3,11,19], and have been predicted by helioseismological models; cf. [9]. The spatial pattern of about 10 Mm, which POD associates with high-frequency modes, is in agreement with the horizontal coherence length attributed to solar p modes. In order to confirm this, we compared the k - ω classical results with the POD spectra. Choosing, for example, the POD mode $j = 12$, we performed a cut of the k - ω spectrum at the measured peak frequency (3254 μHz). We thus obtain a wavelength spectrum, reported on Fig. 1, that can be compared with the $j = 12$ eigenfunction spectrum. As can be seen, the spikes observed in the POD spectrum qualitatively correspond to the typical ridges structure of the k - ω spectrum.

Concerning the low-frequency dominated modes, it is interesting to note that the measured frequency range, mentioned above, is compatible with the theoretical results on solar gravitational modes [3,9]. However, because of the resolution limit, related to the finite length of the time series, the low-frequency oscillations detected by POD cannot be unambiguously attributed to discrete modes, rather than to a continuum. The evidence of center-limb modulation shows that such modes are mainly associated with the contribution of horizontal velocities. To confirm this, we tried to apply the POD technique to a reduced square of about 100×100 pixels taken at the center of each image, where horizontal components of the velocity are weaker. In this case, the low-frequency oscillations are no longer observed (see Fig. 4). As for the p modes, the k - ω cut can be performed at the peak frequency of, for example, mode $j = 8$ (76 μHz). The comparison with the POD eigenfunction wavelength spectrum is shown in Fig. 1, and again reveals a qualitative agreement between the two techniques. The characteristic integral scale computed for the k - ω cut is also in agreement with the corresponding POD integral scale. Since the POD basis functions are not chosen *a priori*, the association between small-scale eigenfunctions and low-frequencies is reliable. In order to test this, we reduced the resolution of the data by performing a spatial 50×50 pixels running average of the fields before applying POD. In this case, the low-

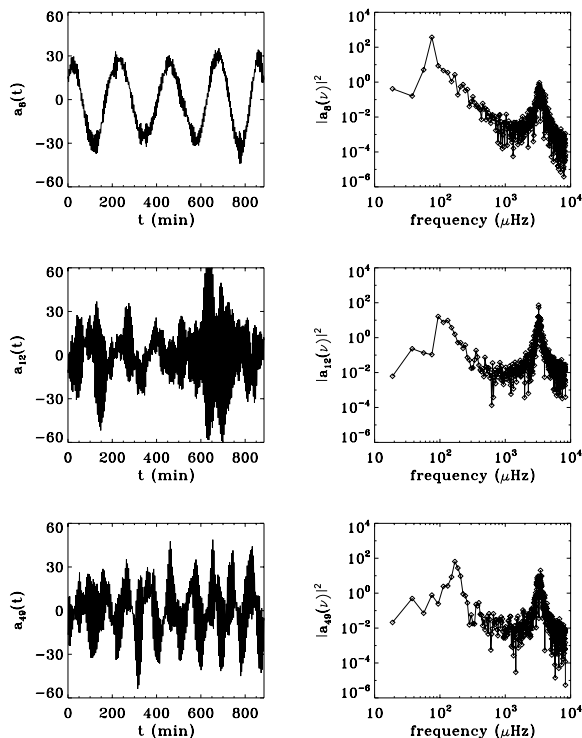


FIG. 3. Left column: time evolution of POD coefficients $a_j(t)$ (m/s) for the same three modes as in Fig. 1. Right column: the corresponding frequency spectra $|a_j(\nu)|^2$ (m^2/s^2).

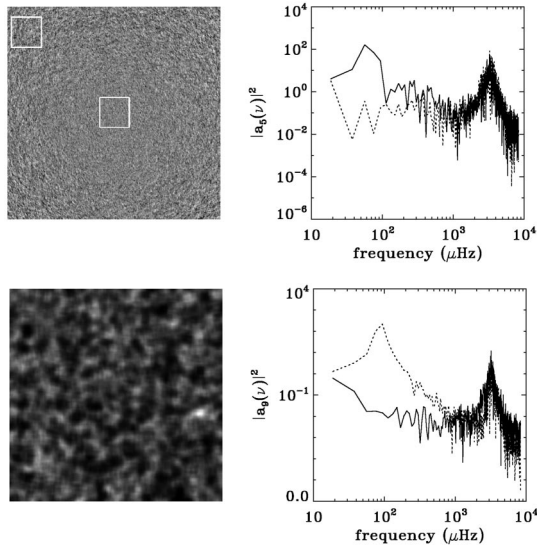


FIG. 4. Upper panels: the POD eigenfunction $\Psi_6(x, y)$ (left, the center-limb modulation is evident) and the Fourier spectra (right) obtained from two reduced square boxes of size 100×100 pixels, taken at the center (dotted line) and at the border (full line) of the image (see left panel). Bottom panels: 50×50 pixels running averaged data at a given time (left), and the $j = 9$ POD mode wave vector spectrum (right) for both the smoothed field (full line) and the original field (dotted line).

frequency peaks in the coefficient spectra are completely lost (see Fig. 4).

In conclusion, we presented the first application of POD on high resolution solar photospheric velocity fields, which represents an example of convective turbulence in high Rayleigh numbers natural fluids. POD is able to capture the main energetic and spatial features of the solar photosphere. In particular, the dynamical processes of interest are automatically separated from the most energetic but uninteresting mode which captures solar rotation. Two main oscillatory processes, well separated in frequency, are detected in all the other modes: high-frequency oscillations in the range $3250\text{--}3550 \mu\text{Hz}$ and low-frequency oscillations in the range $20\text{--}130 \mu\text{Hz}$. The high-frequency waves are the well-known acoustic p modes and their properties, as obtained from POD, are in agreement with previous results based on Fourier techniques. On the other hand, low-frequency oscillations, with frequencies compatible with those expected from the theory of solar g modes, prevail in the most energetic POD modes (excluding solar rotation), which are characterized by spatial eigenfunctions with typical scales of ≈ 3 Mm. The clear association between low-frequency oscillations and small spatial scales, which are close to the solar granulation, is the most interesting and most surprising result provided by our analysis. This suggests the presence of a strong coupling between low-frequency modes and the turbulent convection, which could have implications on the inversion

of time-distance measurements of sound waves [20], also used to infer the properties of the turbulent convection below the surface. Such coupling could be related to the dishomogeneities and small-scale structures arising from the highly nonlinear dynamics of the convective layers. This point needs to be investigated in future theoretical studies. A further improvement of this analysis can be expected from its application to longer time series.

We acknowledge useful discussions with A. Mangeney. Th. S. was supported by MIUR.

-
- [1] T. S. Akhromeyeva *et al.*, Phys. Rep. **176**, 189 (1989); M. I. Rabinovich, A. B. Ezersky, and P. D. Weidman, *The Dynamics of Patterns* (World Scientific, Singapore, 2000).
 - [2] R. J. Bray, R. E. Loughhead, and C. J. Durrant *The Solar Granulation* (Cambridge University Press, Cambridge, England, 1984).
 - [3] M. Stix, *The Sun: An Introduction* (Springer-Verlag, Berlin, 2002).
 - [4] R. F. Stein and A. Nordlund, *Astrophys. J.* **342**, L95 (1989); H. C. Spruit, A. Nordlund, and A. M. Title, *Annu. Rev. Astron. Astrophys.* **28**, 263 (1990).
 - [5] R. B. Leighton, R. W. Noyes, and G. W. Simon, *Astrophys. J.* **135**, 474 (1962).
 - [6] M. Rieutord *et al.*, *Astron. Astrophys.* **357**, 1063 (2000).
 - [7] L. E. Cram, B. R. Durney, and D. B. Guenther, *Astrophys. J.* **267**, 442 (1983).
 - [8] J. R. Brookes, G. R. Isaak, and H. B. von der Raay, *Nature (London)* **259**, 92 (1978); A. B. Severny, V. A. Kotov, and T. T. Tsap, *Nature (London)* **259**, 87 (1976); D. J. Thomson, C. G. MacLennan, and L. J. Lanzerotti, *Nature (London)* **376**, 139 (1995).
 - [9] J. Cristensen-Dalsgaard, *Rev. Mod. Phys.* **74**, 1073 (2002).
 - [10] R. K. Ulrich, *Astrophys. J.* **162**, 993 (1970).
 - [11] F.-L. Deubner, *Astron. Astrophys.* **39**, 31 (1974); **44**, 371 (1975).
 - [12] G. Berthomieu and J. Provost, *Astron. Astrophys.* **227**, 563 (1990); O. Andraess, B. N. Andersen, and C. E. Wasberg, *Astron. Astrophys.* **257**, 763 (1992); T. Appourchaux *et al.*, *Astrophys. J.* **538**, 401 (2000).
 - [13] P. D. Mininni, D. O. Gómez, and G. B. Mindlin, *Phys. Rev. Lett.* **89**, 061101 (2002).
 - [14] P. Holmes, J. L. Lumley, and G. Berkooz, *Turbulence, Coherent Structures, Dynamical Systems and Symmetry* (Cambridge University Press, Cambridge, England, 1996).
 - [15] SOHO is a mission of international cooperation ESA-NASA. MDI is supported by OSS/NASA.
 - [16] Th. Straus, G. Severino, F.-L. Deubner, B. Fleck, S. M. Jefferies, and T. Tarbell, *Astrophys. J.* **516**, 939 (1999).
 - [17] G. Alfonsi and L. Primavera, *Journal of Flow Visualization and Image Processing* **9**, 89 (2002).
 - [18] S. B. Pope, *Turbulent Flows* (Cambridge University Press, Cambridge, England, 2000).
 - [19] J. W. Leibacher, R. W. Noyes, J. Toomre, and R. K. Ulrich, *Sci. Am.* **253**, No. 3, 34 (1985).
 - [20] T. L. Duvall, S. M. Jefferies, J. W. Harvey, and M. A. Pomerantz, *Nature (London)* **362**, 430 (1993).